Article

Investigation of the Pressure Fluctuation of Piston Chambers with Variable Slot Geometry

Dongyun Wang [1,2], Congcong Chen [1] and Hongkang Dong [1,*]

1   College of Engineering, Zhejiang Normal University, Jinhua 321004, China
2   Key Laboratory of Urban Rail Transit Intelligent Operation and Maintenance Technology & Equipment of Zhejiang Province, Jinhua 321000, China
*   Correspondence: dong_hk@zjnu.edu.cn; Tel.: +86-188-1135-8957

Abstract: High-pressure fluctuation and flow ripple may cause unexpected vibration and noise when the piston pump works under severe conditions, and eventually lead to hydraulic transmission failure. The geometry of the valve plate has a great influence on the pressure fluctuation of the piston chamber. In order to optimize the structure of the valve plate, a mathematical model considering the slot geometry and the flow leakage of the lubricating interfaces was established in this paper. The model was used to investigate the pressure of the piston chamber, and then the accuracy of the model was validated by comparing simulation and experimental results. Further simulation results show that the pressure fluctuation in the piston chamber can be effectively suppressed by optimizing the triangular slots parameter of the valve plate, and a good design of the slot geometry could reduce the undershoot and overshoot of the pressure in piston chamber at the starting moment.

Keywords: piston pump; pressure fluctuation; valve plate; triangular slot

1. Introduction

The axial piston pump is in widespread use for the advantages of compact structure, high power density, and high volumetric efficiency [1,2]. On the contrary, the noise and cavitation are the drawbacks limiting its application in extreme working conditions and affecting its lifetime. The noise and cavitation have been traced back to the improper design of the valve-plate slots within the pump [3–6]. Therefore, it is of great significance to investigate the pressure fluctuation of piston chambers with variable slot geometry and multiple working conditions [7].

Peer researchers carried out theoretical analysis with the help of CFD technologies and a simplified test bench. Bergada [8] considered a CFD analytical approach toward the understanding of the hydrostatic leakage and lifted characteristic of a flat-type slipper within an axial piston pump. Zhang [9] studied the flow ripple characteristics of an axial piston pump by using CFD technology. Vacca et al. [10] studied the cavitation in hydraulic pumps by lumped parameter method and CFD method. Jiang et al. [11] proposed a numerical model of the piston/cylinder interface to investigate the chamber and groove's influence on the film characteristics. In the later study, the group presented a comprehensive numerical simulation method to study slipper microstructures on the lubrication performance of the slipper-swashplate interface [12]. Zhao [13] analyzed the transient evolution of the submerged cavitation jet in an axial piston pump with a spherical valve plate from the perspectives of pressure, velocity, and gas volume fraction change using CFD simulation tools. Fang et al. [14] established a CFD model based on the full cavitation model (FCM) to simulate the flow field of the axial piston pump and set up a test rig to verify the model. Chao et al. [15] developed a computational fluid dynamics model to compare the pump flow characteristics between a standard piston and a capped piston. The simulation results show that the capped piston can significantly reduce the

compressibility effect, pressure fluctuation, and cavitation under a wide range of working conditions compared with the standard hollow piston.

The pressure fluctuation, flow ripple, and noise originating from the piston pump are usually caused by the improper design of the valve plate structure, and many scholars have performed a large number of studies to optimize the pump structures. Manring [16] explored the advantages of using various valve-plate slot geometries within an axial piston pump. The results revealed that applying quadratically varying slot geometry is not reasonable since it had no obvious effect on improving the performance. Johansson et al. [17] optimized the cross-angle of the swash plate to reduce the noise in piston pumps via a simulation model and verified the applicability of the model through experiments. Ivantysynova [18] found that the pressure fluctuation, forces applied on the swash plate, and the control stability of the swash plate was directly related to the rate of pressurization and decompression of the piston chamber. Further investigations [19–21] compared the effectiveness of several passive design methods for reducing the pump noise by a computer-aided multi-objective optimization procedure. Wang [22] used the important concept of pressure carryover to establish the mathematical relationship between the geometry of the valve plate and the volumetric efficiency of the piston pump. Xu et al. [23,24] improved the single-cylinder and multi-cylinder pumping dynamics model of a swash plate piston pump, proposed a design method of valve plate based on flow area matching and transient backflow reduction, and optimized the valve plate transition region accordingly. The results showed that the application of this design method is effective in reducing flow ripple and eliminating pressure overshoot and undershoot. In 2016, the research group continued to study how to reduce the flow ripple of the axial piston pump through the combination of cross-angle and pressure relief grooves [25]. Ye et al. [26] developed a dynamic pump model considering air release and cavitation and optimized the valve plate. At present, most scholars use theoretical calculations or simulation technology to obtain the dynamic changes of the discharge pressure. However, the research on the factors affecting the pressure change in the piston chamber is still not enough. In previous studies, the transition slot is assumed to be a specific geometry, and the detailed effect of different slot shapes needs to be further investigated.

This paper aims to study the influence of outlet pressure, shaft speed, and valve-plate slot geometries on the pressure fluctuation in the piston chamber in order to analyze the factors that cause the pressure transient behavior in the piston chamber. First, a mathematical model of the piston pump was developed considering the variable flow area of the valve plate and leakage flow through the lubricating interfaces. Second, the experiment tests were conducted, and the model was verified under different operational speeds. Lastly, the effect of slot geometry was discussed through further simulation results.

2. Mathematical Model

2.1. Modelling of the Kinematic of the Pistons

Figure 1 shows the kinematic diagram of the swash plate axial piston pump. As the drive shaft rotates, it causes the pistons to reciprocate within the cylinder block bores. The piston shoes are held against a bearing surface by compression force during the discharge stroke and by the shoe hold-down plate and retainer during the intake stroke. The bearing surface of the piston shoe is held at an angle to the drive shaft axis of rotation by the swashplate.

In this study, the outer dead center (ODC), where the piston chamber is at the maximum volume, is defined as the initial point ($\varphi = 0°$). Therefore, the piston displacement L can be obtained from the axial distance between ODC and A point.

$$L = -R \tan \beta (1 - \cos \varphi) \tag{1}$$

where R is the cylinder pitch radius, β is the inclination angle of the swash plate, φ is the angle of the piston relative to the outer dead center ($\varphi = \omega t$), ω is the angular velocity, and t is the time.
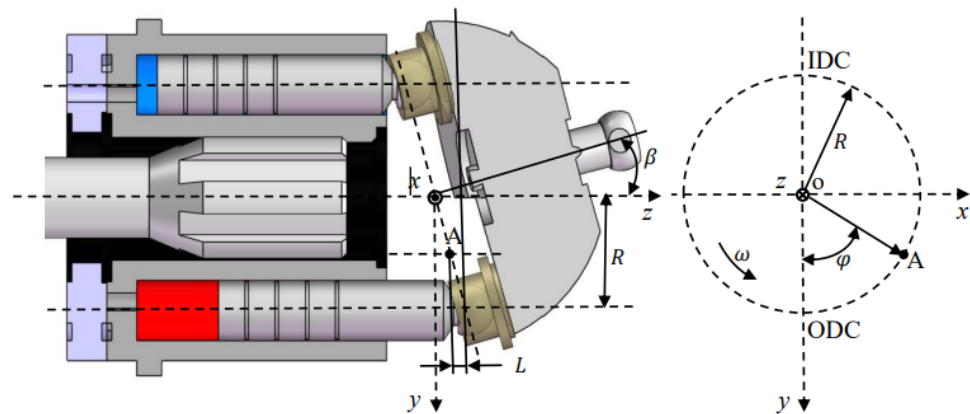
Figure 1. Kinematic diagram of swash plate axial piston pump.

Since the piston also rotates around the shaft, its circumferential velocity u can be obtained by the following equation:

$$u = \omega R \tag{2}$$

The axial velocity of the piston v can be obtained by the first-order derivative of the piston displacement with respect to the time.

$$v = \frac{dL}{d\varphi}\frac{d\varphi}{dt} = -\omega R \tan\beta \sin\varphi \tag{3}$$

The axial acceleration of the piston a can be obtained by the second-order derivative of the piston displacement with respect to the time:

$$a = \frac{dv}{d\varphi}\frac{d\varphi}{dt} = -\omega^2 R \tan\beta \cos\varphi \tag{4}$$

2.2. Modelling of the Valve plate Opening Area

The main structure of the valve plate includes the inner and outer sealing belt, the kidney groove for oil suction and discharge, and the transition zone structure. The oil film of the inner and outer sealing belt determines the bearing capacity, friction, and wear performance of the valve plate. The piston is alternately connected with the low-pressure port and the high-pressure port to form the suction and discharge process of the axial piston pump.

From Figure 2, we can see that when the piston pump is working, the oil flows into or out of the piston chamber through the kidney of the valve plate. When the piston chamber is connected with the damping hole on the groove, the throttling effect will be intensified. The flow area S is affected by the relative position of the piston chamber and the valve plate notch.

As shown in Figure 2a, the piston chamber is connected with the suction and discharge port of the valve plate successively with the rotation of the shaft. When the piston chamber connects to the triangular slot of the valve plate, the flow area has the characteristics of the minimum area, and the cross-section is perpendicular to the streamline. The minimum flow area S_{min} at the "*bc*" position is the area of Δbcd in the figure:

$$S_{min} = \frac{1}{2}bc \cdot h = R^2 \cdot \Delta\varphi^2 \cdot \sin\theta_1 \cdot \tan\theta_1 \cdot \tan\frac{\theta_3}{2} \tag{5}$$

where $bc = 2R\Delta\varphi \tan\theta_1 \tan\frac{\theta_3}{2}$, $h = R\Delta\varphi \sin\theta_1$, θ_1 is the depth angle of the transverse section of the triangular vibration damping groove, θ_2 is the width angle of the transverse section of the triangular vibration damping groove, and θ_3 is the width angle of the longitudinal section of the triangular vibration damping groove.
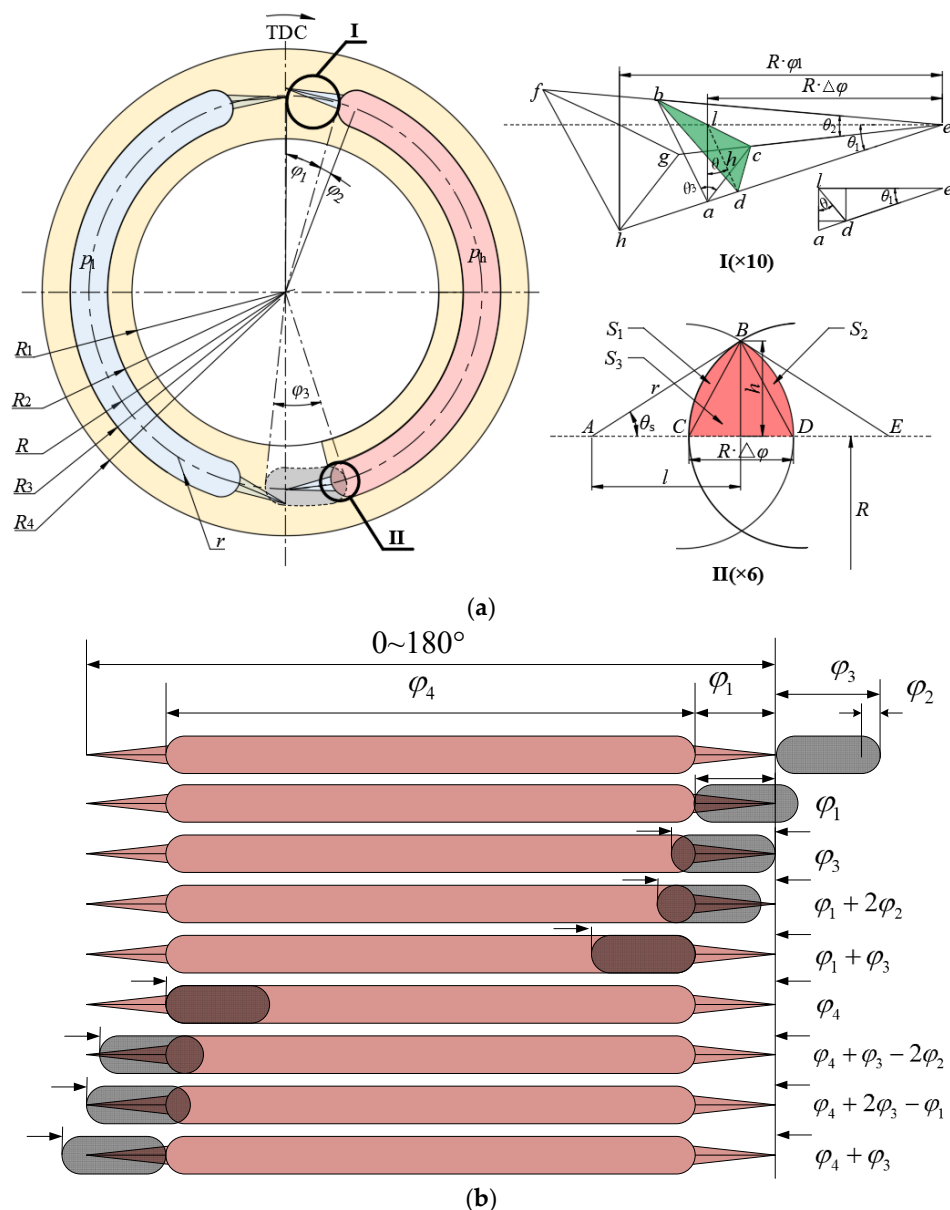
Figure 2. Schematic diagram of flow area: (**a**) Structure of piston chamber and the port window of value plate and its partially enlarged view; (**b**) Schematic diagram of piston chamber and value plate port window position.

As shown in the partially enlarged view, when the piston chamber is at the crossing position with the end of the high and low-pressure distribution window, the area of the shaded part in the figure is half of the flow area. Based on the geometric relationship, it can be seen that the area of the shaded part (S_S) is equal to the sum of two equal arch areas (S_1 and S_2) and the area of an isosceles triangle (S_3). The calculation is as follows:

$$S_S = 2(S_1 + S_2 + S_3) \tag{6}$$

where $S_1 = S_2 = \frac{1}{2}r^2\theta_s - \frac{1}{2}rh$, $S_3 = \frac{1}{2}\Delta\varphi \cdot R \cdot h$
$\theta_s = \arccos\frac{l}{r} = \arccos(\frac{2r-\Delta\varphi R}{2r})$, $h = \sqrt{r^2 - l^2} = \sqrt{r^2 - (\frac{2r-\Delta\varphi R}{2})^2}$, r is the radius of start-

ing and ending circles of the kidney groove.

We can observe from Figure 2b that the connection of the piston chamber and valve plate can be divided into eight stages within the range of 0 to 180° shaft rotation angle.

Since the geometry of the valve plate studied in this paper is completely symmetrical, only the stages within 0 to 180° are necessary to be presented. The calculation is shown in Table 1:

Table 1. Specific calculations of the valve plate opening area.

Position	Expression
$(0, \varphi_1]$	$S = R \cdot r \cdot \varphi \cdot \sin\theta_1 \cdot arc\tan(R \cdot \varphi \cdot \tan\theta_1 \cdot \tan\frac{\theta_3}{2}/r)$
$(\varphi_1, \varphi_3]$	$[(\varphi - \varphi_1)R - 2r]\sqrt{(\varphi - \varphi_1)Rr - \frac{1}{4}(\varphi - \varphi_1)^2 R^2} + 2r^2\arccos\left[\frac{2r - (\varphi - \varphi_1)R}{2r}\right] + S(\varphi = \varphi_1)$
$(\varphi_3, \varphi_1 + 2\varphi_2]$	$S(\varphi = \varphi_1) - R \cdot r \cdot (\varphi - \varphi_3) \cdot \sin\theta_1 \cdot arc\tan(R \cdot (\varphi - \varphi_3) \cdot \tan\theta_1 \cdot \tan\frac{\theta_3}{2}/r)$ $+[(\varphi - \varphi_3)R - 2r]\sqrt{(\varphi - \varphi_3)Rr - \frac{1}{4}(\varphi - \varphi_3)^2 R^2} + 2r^2\arccos\left[\frac{2r - (\varphi - \varphi_3)R}{2r}\right]$
$(\varphi_1 + 2\varphi_2, \varphi_1 + \varphi_3]$	$S(\varphi = \varphi_1) - R \cdot r \cdot (\varphi - \varphi_1 - 2\varphi_2) \cdot \sin\theta_1 \cdot arc\tan(R \cdot (\varphi - \varphi_1 - 2\varphi_2) \cdot \tan\theta_1 \cdot \tan\frac{\theta_3}{2}/r)$ $+\pi r^2 + (\varphi - \varphi_1 - 2\varphi_2) \cdot R \cdot 2r$
$(\varphi_1 + \varphi_3, \varphi_4]$	$\pi r^2 + (\varphi_1 - 2\varphi_2) \cdot R \cdot 2 \cdot r$
$(\varphi_4, \varphi_4 + \varphi_3 - 2\varphi_2]$	$S(\varphi = \varphi_1) - R \cdot r \cdot (180 - \varphi) \cdot \sin\theta_1 \cdot arc\tan(R \cdot (180 - \varphi) \cdot \tan\theta_1 \cdot \tan\frac{\theta_3}{2}/r)$ $+\pi r^2 + (\varphi - \varphi_4) \cdot R \cdot 2r$
$(\varphi_4 + \varphi_3 - 2\varphi_2,$ $\varphi_4 + 2\varphi_3 - \varphi_1]$	$S(\varphi = \varphi_1) - R \cdot r \cdot (\varphi - \varphi_4 - \varphi_3 + 2\varphi_2) \cdot \sin\theta_1 \cdot arc\tan(R \cdot (\varphi - \varphi_4 - \varphi_3 + 2\varphi_2) \cdot \tan\theta_1 \cdot \tan\frac{\theta_3}{2}/r)$ $+[(\varphi - \varphi_4 - \varphi_3 + 2\varphi_2)R - 2r]\sqrt{(\varphi - \varphi_4 - \varphi_3 + 2\varphi_2)Rr - \frac{1}{4}(\varphi - \varphi_4 - \varphi_3 + 2\varphi_2)^2 R^2}$ $+2r^2\arccos\left[\frac{2r - (\varphi - \varphi_4 - \varphi_3 + 2\varphi_2)R}{2r}\right]$
$(\varphi_4 + 2\varphi_3 - \varphi_1,$ $\varphi_4 + \varphi_3]$	$[(\varphi - \varphi_4 - 2\varphi_3 + \varphi_1)R - 2r]\sqrt{(\varphi - \varphi_4 - 2\varphi_3 + \varphi_1)Rr - \frac{1}{4}(\varphi - \varphi_4 - 2\varphi_3 + \varphi_1)^2 R^2}$ $+2r^2\arccos\left[\frac{2r - (\varphi - \varphi_4 - 2\varphi_3 + \varphi_1)R}{2r}\right] + S(\varphi = \varphi_1)$

2.3. Modelling of the Inlet and Outlet Flow

The piston pump has z pistons uniformly distributed in the cylinder block bores and the piston angular gap $\alpha = 2\pi/z$. There are *i* pistons connected to the oil discharge chamber at the same time at different shaft angles φ, so the instantaneous theoretical delivery rate Q is a period of $\alpha/2$. The expression of Q within the range of $(0 \sim \alpha)$ is shown in Equation (7).

$$
\begin{aligned}
Q &= \sum_1^i S_k v_k = \frac{\pi}{4} R_k{}^2 \omega R \tan\beta \sum_1^i \sin[\varphi + (i-1)\alpha] \quad i = \begin{cases} \frac{z+1}{2} & 0 < \varphi < \frac{\alpha}{2} \\ \frac{z-1}{2} & \frac{\alpha}{2} < \varphi < \alpha \end{cases} \\
&= \frac{\pi}{8} R_k{}^2 \omega R \tan\beta \frac{\cos\left[\varphi - \frac{\alpha}{2} + (-1)^{k+1}\frac{\alpha}{4}\right]}{\sin\left(\frac{\alpha}{4}\right)} \quad k = \begin{cases} 1 & 0 \le \varphi < \frac{\alpha}{2} \\ 2 & \frac{\alpha}{2} \le \varphi < \alpha \end{cases}
\end{aligned}
\tag{7}
$$

Based on the principle of mass conservation in the control volume, the differential equation of pressure at the inlet and outlet port of the piston pump can be expressed as:

$$
\begin{cases}
\frac{dp_h}{dt} = \frac{K}{V_h}\left(q_{back,hp} - q_{out} - q_{leak,hp}\right) \\
\frac{dp_l}{dt} = \frac{K}{V_l}\left(q_{back,lp} - q_{in} - q_{leak,lp}\right)
\end{cases}
\tag{8}
$$

where V_h and V_l are the volumes of the outlet and inlet pipeline, $q_{leak,hp}$ and $q_{leak,lp}$, are the leakage flows of the high and low-pressuree port of the valve plate, K is volume modulus, see Equation (15) for details.

$q_{\text{back,hp}}$ represents the sum of the backflow of all piston chambers connected with the high-pressure port of the valve plate, while $q_{\text{back,lp}}$ represents the backflow connected with the low-pressure port of the valve plate:

$$\begin{cases} q_{\text{back,hp}} = \sum\limits_{i=1}^{z} q_{\text{back,hp},i} \\ q_{\text{back,lp}} = \sum\limits_{i=1}^{z} q_{\text{back,lp},i} \end{cases} \tag{9}$$

The load can be regarded as a throttle valve, and the flow through the throttle is assumed to be turbulence. Therefore, the pump outlet flow q_{out} and the pump inlet flow qin can be expressed:

$$\begin{cases} q_{\text{out}} = C_r S_{\text{hp}} \sqrt{\dfrac{2|\Delta p_{\text{hp}}|}{\rho}} \cdot \text{sign}(\Delta p_{out}) \\ q_{\text{in}} = C_r S_{\text{lp}} \sqrt{\dfrac{2|\Delta p_{\text{lp}}|}{\rho}} \cdot \text{sign}(\Delta p_{in}) \end{cases} \tag{10}$$

where Δp_{hp} is the pressure difference of the orifice at the high-pressure port, which is equal to the load pressure minus the pressure at the high-pressure port, $\Delta p_{\text{hp}} = p_{\text{load}} - p_{\text{h}}$. Δp_{lp} is the pressure difference of the orifice at the low-pressure port, which is equal to the pressure at the inlet pipe minus the pressure at the low-pressure port, $\Delta p_{\text{lp}} = p_{\text{in}} - p_{\text{l}}$. To simplify the calculation, the pressure difference can be set according to the actual throttling effect of the orifice, which is set as 1 MPa here.

Based on the calculation of the basic structure of the pump $nQ_{\text{t}}/C\sqrt{\frac{2}{\rho}|\Delta p|}$, the high-pressure port throttling cross-sectional area S_{hp} and the low-pressure port throttling cross-sectional area S_{lp} can be determined by the coefficients $K_{\text{area,hp}}$ and $K_{\text{area,lp}}$:

$$\begin{cases} S_{\text{hp}} = K_{\text{area,hp}} \dfrac{nQ_t}{C\sqrt{\frac{2}{\rho}|\Delta p_{out}|}} \\ S_{\text{lp}} = K_{\text{area,lp}} \dfrac{nQ_t}{C\sqrt{\frac{2}{\rho}|\Delta p_{in}|}} \end{cases} \tag{11}$$

where n is the rotational speed, Q_t is the theoretical displacement of the piston pump, C is the discharge coefficient, and ρ is the fluid density.

2.4. Flow Continuity Equation of the Piston Chamber

The coupling of the instantaneous pressure changes of multiple piston chambers forms the pressure fluctuation phenomenon at the pump outlet, so it is necessary to establish a flow model for each piston chamber. Meanwhile, since the fluid viscosity has a great impact on the leakage of the piston pump, and the internal leakage will further affect the outlet pressure fluctuation characteristics, it is also necessary to establish the leakage model at the three lubricating interfaces.

As illustrated in Figure 3, the piston chamber is connected with the flow distribution ports at different angular positions of the valve plate. Considering the flow in/out through the flow distribution port (flow in when connected with the low-pressure port, flow out when connected with the high-pressure port), the leakage flow of cylinder block/valve plate interface, the leakage flow of piston/cylinder interface and the leakage flow of slipper/swash plate interface, the pressure fluctuation model of piston chamber are established.

According to the law of conservation of mass, the change in the product of volume and density caused by compression or expansion is equal to the total mass of outflow and inflow.

$$\sum \dot{m} = \frac{\text{d}}{\text{d}t}(V_{\text{c}}\rho) \tag{12}$$

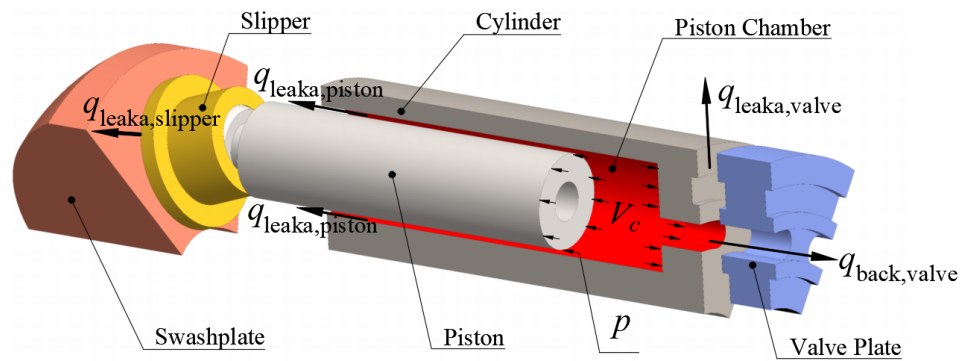where V_{c} is the volume of oil in the piston chamber.

Figure 3. Flow balance diagram of the piston chamber.

The change of mass with respect to time can be derived from the total differential form of volume and density.

$$\frac{\mathrm{d}}{\mathrm{d}t}(V_c \rho) = V_c \frac{\mathrm{d}\rho}{\mathrm{d}t} + \rho \frac{\mathrm{d}V_c}{\mathrm{d}t} \tag{13}$$

Therefore, the change of density with respect to time can be expressed as:

$$\frac{\mathrm{d}\rho}{\mathrm{d}t} = \frac{\rho}{K} \frac{\mathrm{d}p}{\mathrm{d}t} \tag{14}$$

where the volume modulus K represents the pressure change associated with the relative volume change.

$$K = \frac{-\mathrm{d}p V_c}{\mathrm{d}V_c} \tag{15}$$

where p is the pressure in the piston chamber.

Substituting Equation (15) into Equation (14), the following equation can be obtained:

$$\frac{\mathrm{d}}{\mathrm{d}t}(V_c \rho) = \rho \left(\frac{V_c}{K} \frac{\mathrm{d}p}{\mathrm{d}t} + \frac{\mathrm{d}V_c}{\mathrm{d}t} \right) \tag{16}$$

Since the hydraulic fluid density varies a little with pressure and temperature, it is assumed that the density is constant in the present study. By replacing the volume change in the piston chamber with the sum of the flows in and out of the piston chamber, the pressure fluctuation model in the piston chamber can be expressed as follows:

$$\frac{\mathrm{d}p}{\mathrm{d}t} = \frac{K}{V_c} \left(-q_{\mathrm{back,valve}} - q_{\mathrm{leaka,piston}} - q_{\mathrm{leaka,slipper}} - q_{\mathrm{leaka,valve}} - \frac{\mathrm{d}V_c}{\mathrm{d}t} \right) \tag{17}$$

where $q_{\mathrm{back,valve}}$ is the backflow when communicating with the high-pressure side or low-pressure side of the valve plate, $q_{\mathrm{leaka,piston}}$ is the leakage flow of the piston/cylinder interface, $q_{\mathrm{leaka,slipper}}$ is the leakage flow of the slipper/swash plate interface, and $q_{\mathrm{leaka,valve}}$ is the leakage flow of the cylinder block/valve plate interface of the piston chamber.

The piston chamber volume V_c is determined by the piston chamber volume $V_{c,\mathrm{top}}$ at the top dead point position, the piston displacement L and the piston section area S_b. Thus, V_c can be obtained by the following equation:

$$V_c = v V_b + S_b L \tag{18}$$

Therefore, the change of the cylinder volume with time can be determined by the piston speed v and the piston area S_b, and the Equation (19) can be obtained:

$$\frac{\mathrm{d}V_c}{\mathrm{d}t} = v S_b = -\omega R \tan \beta \sin \varphi S_b \tag{19}$$

The backflow $q_{back,valve}$, when communicating with the high-pressure side or low-pressure side of the valve plate, is equal to the sum of the inverted flow from the high-pressure side and the inverted flow from the low-pressure side.

$$q_{back,valve} = q_{back,valve,hp} + q_{back,valve,lp} \tag{20}$$

$$q_{back,valve,hp} = C.S_{hp}\sqrt{\frac{2|p - p_{hp}|}{\rho}} \cdot sign\left(p - p_{hp}\right) \tag{21}$$

$$q_{back,valve,lp} = C.S_{lp}\sqrt{\frac{2|p - p_{lp}|}{\rho}} \cdot sign\left(p - p_{lp}\right) \tag{22}$$

where C is the discharge coefficient, the sign function is defined: $x > 0$, $sign(x) = 1$; $x = 0$, $sign(x) = 0$; $x < 0$, $sign(x) = 1$. As shown in Figure 4, the leakage flow $q_{leake,piston}$ of the piston/cylinder interface can be deduced based on the flow equation of the eccentric cylinder annular gap:

$$q_{leake,piston} = \frac{2\pi R_p h_p{}^3}{8.6817\mu L_f}(p - p_{case}) - 2\pi R_p h_p v \tag{23}$$

where R_p is the piston radius, h_p is the average film thickness of the piston/cylinder interface, μ is the dynamic viscosity of oil, L_f is the coupling length of the piston/cylinder interface, p_{case} is the housing pressure of the piston pump.
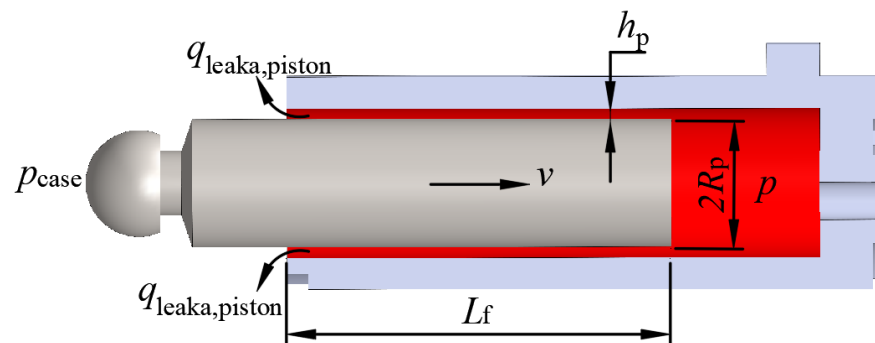

Figure 4. Schematic diagram of leakage flow of piston/cylinder interface.

As shown in Figure 5, the leakage flow $q_{leake,slipper}$ of the slipper/swash plate interface can be deduced based on the equation of the slit flow of parallel plate:

$$q_{leake,slipper} = \frac{\pi d_d{}^4 h_s{}^3}{\mu[6d_d{}^4 \ln(d_{out}/d_{in}) + 128h_s{}^3 l_d]}(p - p_{case}) \tag{24}$$

where d_d is the diameter of the damping hole of the piston ball head, h_s is the average film thickness of the slipper/swash plate interface, d_{out} is the outer diameter of the slipper sealing belt, d_{in} is the inner diameter of slipper sealing belt, l_d is the length of damping hole of the piston ball head.

As is Shown in Figure 6, based on the gap flow formula of the parallel plate, the gap leakage flow $q_{leaka,valve}$ between cylinder block/valve plate interface, can be deduced as follows:

$$q_{leaka,valve} = \frac{\varphi_3 h_v{}^3}{12\mu}\left[\frac{1}{\ln(R_2/R_1)} + \frac{1}{\ln(R_4/R_3)}\right](p - p_{case}) \tag{25}$$

where h_v is the average film thickness of cylinder block/valve plate interface.

The leakage flow of the high-pressure port and the low-pressure port of the valve plate are $q_{\text{leaka,hp}}$ and $q_{\text{leaka,lp}}$, respectively:

$$\begin{cases} q_{\text{leaka,hp}} = \sum\limits_{i=1}^{m} q_{\text{leaka,i}} \\ q_{\text{leaka,lp}} = \sum\limits_{i=1}^{z-m} q_{\text{leaka,i}} \end{cases} \tag{26}$$

where Z is the number of pistons, and m is the number of piston chambers connected with the discharge port of the valve plate:
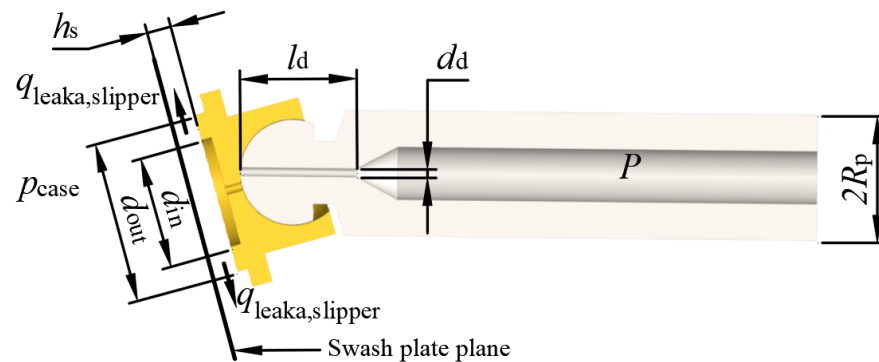

Figure 5. Schematic diagram of leakage flow of slipper/swash plate interface.
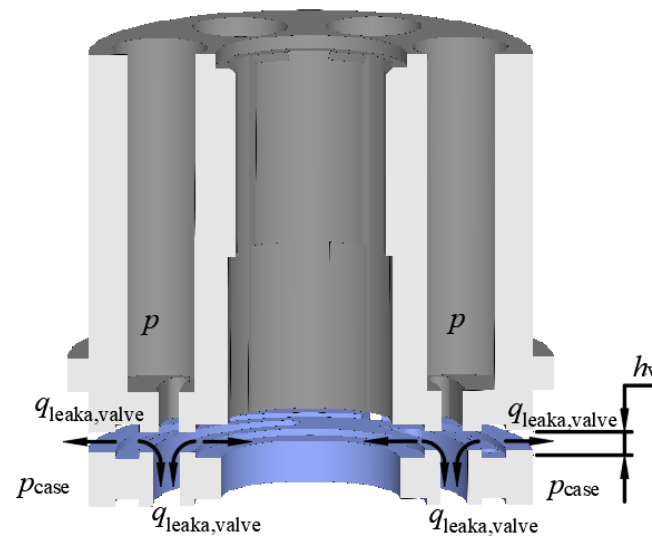
Figure 6. Schematic diagram of leakage flow of the cylinder block/valve plate interface.

2.5. Solution of the Pressure Fluctuation Model

The solution steps of the pressure fluctuation model of the piston chamber are presented in Figure 7. It can be divided into three steps: Firstly, based on the sectional flow area S of the cylinder block/valve plate interface, the pressure of the piston chamber without considering flow ripple at the inlet and outlet of the piston pump is solved. Then, based on the obtained pressure, the inlet and outlet pressures p_h and p_l of the piston pump are solved through the inlet and outlet flow model. Finally, based on the inlet and outlet pressure of the piston pump, the flow entering/exiting through the distribution port, the leakage flow $q_{\text{leak,valve}}$ of the cylinder block/valve plate interface, the leakage flow $q_{\text{leak,piston}}$ of the piston/cylinder interface and the leakage flow $q_{\text{leak,slipper}}$ of the slipper/swash plate interface are calculated, and then the pressure of the piston chamber considering the flow ripple at the inlet and outlet of the piston pump is solved. In this study, the algorithm

was programmed in Matlab. A 12 GB RAM computer with an Intel i7-9750H @2.60GHz processor was employed for the simulation.
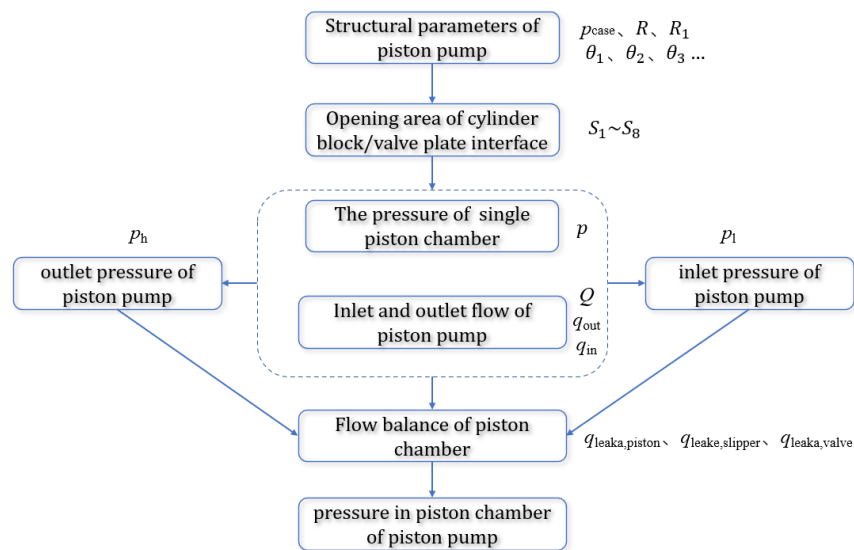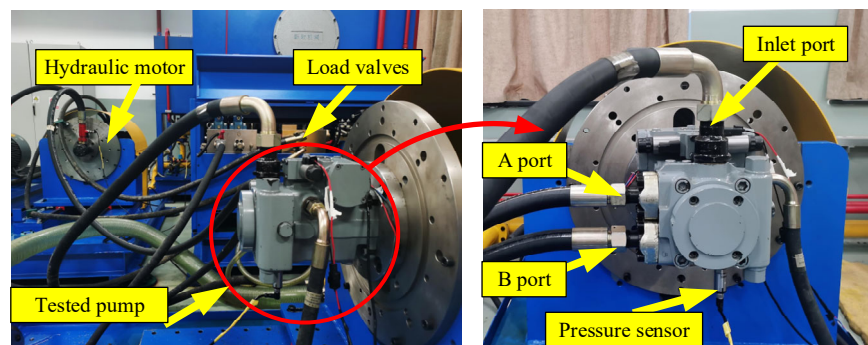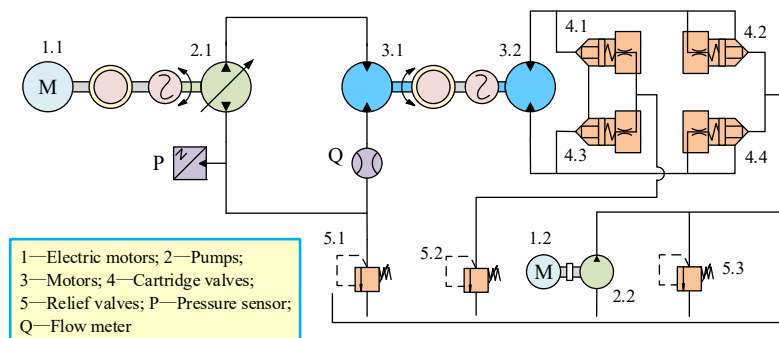

Figure 7. Flow chart of solving pressure fluctuation model of the piston chamber.

3. Experiments and Validation

In order to verify the numerical model, a swashplate-type piston pump was tested in a closed-circuit hydraulic system shown in Figure 8. The measured parameters of the piston pump are shown in Table 2. The piston pump, produced by Hytek Hydraulic, is driven by a 75 kW variable frequency motor, and its rotational speed can be regulated from 0 to 1500 r/min.

(a) Experimental setup

1—Electric motors; 2—Pumps;
3—Motors; 4—Cartridge valves;
5—Relief valves; P—Pressure sensor;
Q—Flow meter

(b) Hydraulic schematic

Figure 8. Experimental setup and its schematic.

Table 2. Measured parameters of the piston pump.

| Component	Description	Value
Tested pump	Number of pistons (null)	9
	Pitch radius of pistons (mm)	41.9
	Diameter of piston (mm)	20
	Rated speed (r/min)	3050
Hydraulic fluid	Rated pressure (bar)	400
	Density (20 °C, kg/m^3)	875
	Kinematic viscosity (mm^2/s)	46
	Isentropic bulk modulus (Pa)	1.6×10^9

The ports of the pump are directly connected to the ports of a hydraulic motor, which can adjust the system pressure via a set of cartridge valves. For the measurement of the instantaneous discharge pressure of the tested pump, a piezo-electric ceramics type pressure sensor with high degree accuracy and dynamic response is arranged at one of the outlet ports of the pump.

Additional detailed descriptions of the sensors are listed in Table 3. The accuracy range of measured pressure is $p \pm 3$ bar. Several experimental tests were performed to obtain the instantaneous discharge pressure of the tested pump. The hydraulic fluid used in the test rig was hydraulic oil VG46. The temperature of the hydraulic oil was maintained at approximately 50 °C. The unit was tested at different speeds and loads. During the tests, keep the discharge pressure unchanged, and select two typical working conditions: low speed (1000 r/min) and high speed (1500 r/min) for comparative analysis.

Table 3. Main sensors and equipment descriptions.

Sensors	Range	Frequency Response	Accuracy
Speed sensor	0–2000 r/min		0.5% FS
Flow meter	0–500 L/min		0.5% FS
Out pressure sensor	0–600 bar	>3 kHz	0.5% FS

Figure 9 illustrates the comparisons of the discharge pressure between the simulation results and measurements at a discharge pressure of 20 MPa and rotational speed of 1500 r/min. Figure 10 illustrates the comparisons of the discharge pressure between the simulation results and measurements at a discharge pressure of 20 MPa and rotational speed of 1000 r/min.
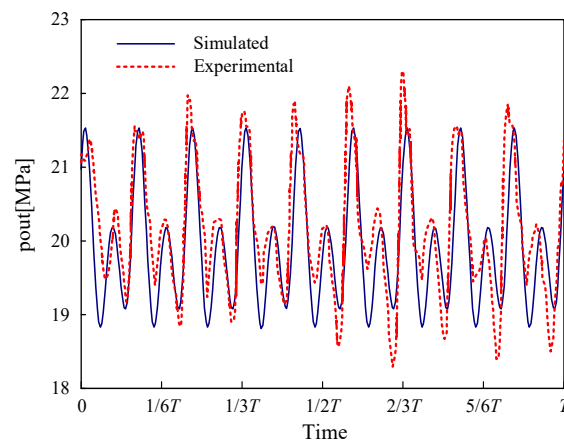
Figure 9. Discharge pressure comparison between the simulated and measured results (under the discharge pressure of 20 MPa and rotational speed of 1500 r/min).
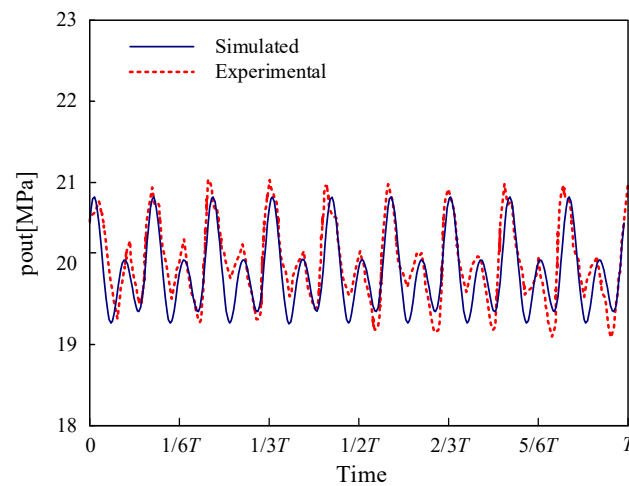
Figure 10. Discharge pressure comparison between the simulated and measured results (under the discharge pressure of 20 MPa and rotational speed of 1000 r/min).

It can be seen from Figures 9 and 10 that the curve of the simulations changes along with the trend of the experimental results, which can verify the accuracy of the mathematical model.

4. Results and Discussions

4.1. Pressure Fluctuation of the Piston Chamber

The pressure fluctuation curve of the piston chamber can be obtained by the numerical model, as shown in Figure 11.
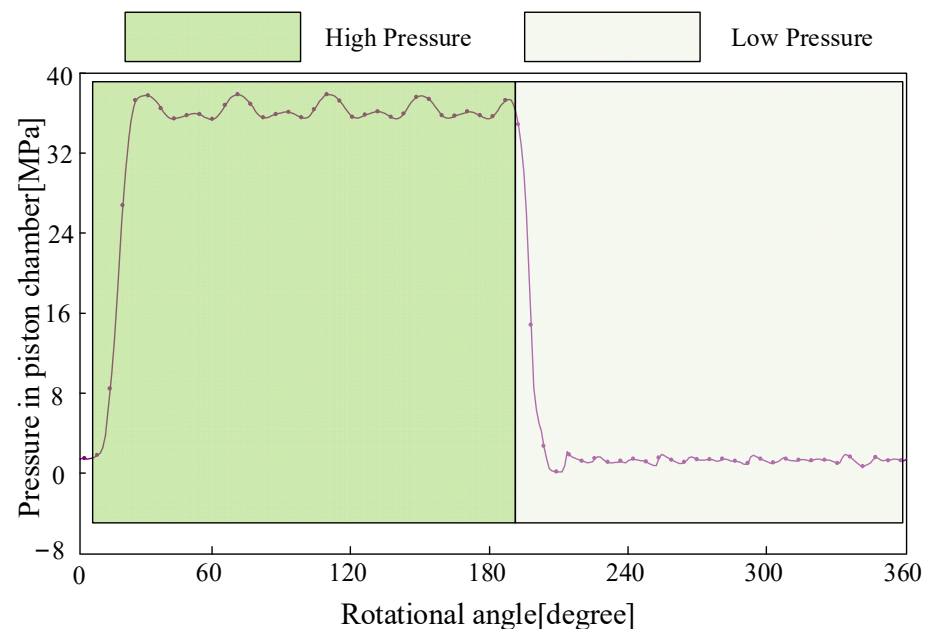

Figure 11. Pressure in piston chamber with constant outlet pressure pout (36 MPa) and constant shaft speed *n* (1500 r/min).

It can be seen from the figure that the pressure fluctuation in the piston chamber changes periodically, with the minimum positive period of 360°, denoted as *T*.

During the first 180° of each cycle, the piston chamber is connected to the high-pressure port of the valve plate (the outlet side of the piston pump), and the amplitude of the outlet pressure fluctuates. During the second 180° of each cycle, the piston chamber is connected

with the low-pressure port of the valve plate (the inlet side of the piston pump), and the pressure of the piston chamber fluctuates accordingly with inlet pressure.

At the shaft angle $\varphi = T + 24°$, since the piston chamber is transformed from a completely closed state to communicate with the triangular groove of the high-pressure port, the pressure of the piston chamber has an overshoot, and the triangular groove at the front end of the high-pressure port is designed to reduce this overshoot.

Similarly, at the shaft rotation angle $\varphi = T + 196°$, the pressure of the piston chamber has a undershoot because the piston chamber changes from a completely closed state to a triangular groove connected to the low-pressure port.

Before the piston chamber connects with the suction of the discharge port of the valve plate, it should enter a transition zone first. If the transition zone of the valve plate is not well designed, the overshoot and undershoot of the pressure in the piston chamber may occur remarkably. At the beginning and end of the suction port, the flow area between the valve plate and piston chamber is quite small. Therefore, the pressure drop during the suction stroke will be significant and eventually lead to pressure undershooting in the piston chamber. Similarly, a pressure overshoot will occur when the piston chamber starts to connect with the discharge port of the valve plate. Such an overshoot could generate instantaneous high pressure, which is far greater than the working pressure.

4.2. Effect of the Slot Geometry

In this section, a comprehensive parametric analysis is carried out to enhance the understanding of the effects of the slot geometry on the pressure fluctuation in the piston chamber. In the parametric analysis, when the effect of slot geometry is studied, the other parameters remain the same. According to a typical triangular groove structure, five groups of slot geometry are listed in Table 4:

Table 4. Parameters related to simulation.

The Combination of Triangular Groove Parameter	G1	G2	G3	G4	G5
Depth angle of the transverse section of triangular vibration damping groove θ_1 (°)	10	10	10	15	5
Width angle of the transverse section of triangular vibration damping groove θ_2 (°)	20	15	25	20	20
Width angle of the longitudinal section of triangular vibration damping groove θ_3 (°)	90.10	74.34	103.86	68.53	127.40

The pressure fluctuation curves of the piston chamber with constant shaft speed (1000 r/min), constant outlet pressure (30 MPa), and variable triangular groove parameter combination G ($\theta_1, \theta_2, \theta_3$) are shown in Figure 12.

In Figure 12, we can see that the five pressure curves show the same tendency as the curve presented in the aforementioned section. For the majority of the time, the piston chamber is connected to the suction/discharge port of the valve plate; hence the pressure profile reflects the suction or discharge pressure fluctuation. In addition, due to the existence of the valve plate slots, there are no significant pressure peaks when the piston chamber is isolated. However, the five pressure curves have different rising and decreasing rates when the piston chamber starts to connect with valve plate ports.

The pressure in the piston chamber of the rising period is shown in Figure 13. It can be seen that: in the region of $(0–24)°$, the rising rate of the rising period from fast to slow is G4 (15, 20, 68.53), G3 (10, 25, 103.86), G1 (10, 20, 90.10), G2 (10, 15, 74.34), G5 (5, 20, 127.40). The higher θ_1 is, the faster the rising rate is, and θ_1 has the most significant effect on the rising rate of the pressure in the piston chamber.
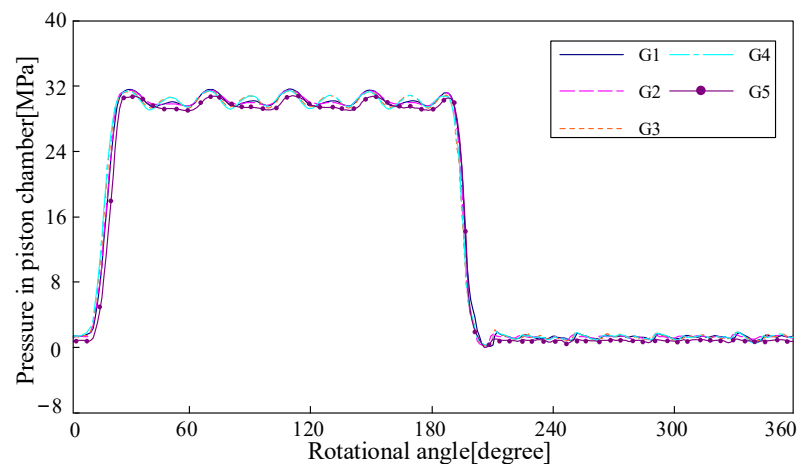
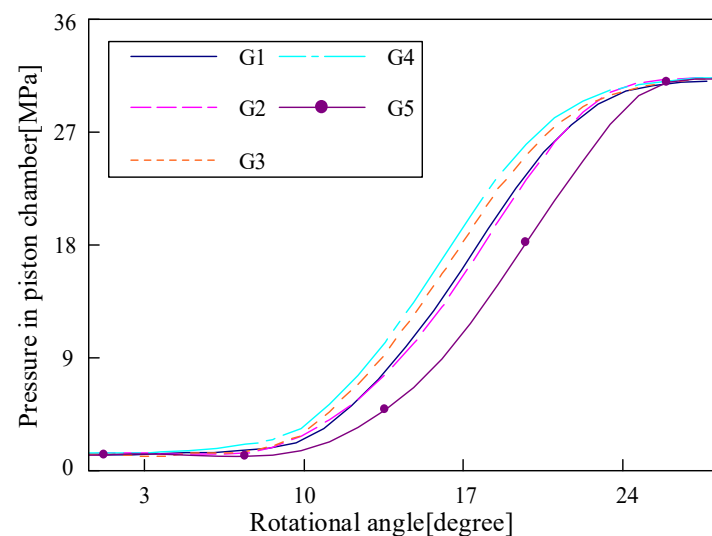**Figure 12.** Pressure in piston chamber with different slot geometries.

Figure 13. Pressure in the piston chamber with different slot geometries at the beginning of the discharge phase.

Focusing on the three groups of triangular groove parameter combinations G1, G2, and G3 with $\theta_1 = 10°$, it can be found that the larger θ_2 is (θ_3 associated with θ_2 also increases), the faster the rising rate. In summary, at this stage, the pressure in the piston chamber changes most gently under the parameters of G5, so the impact effect is also smaller. In real working conditions, under the triangular groove structure with the same volume, it would be better to increase θ_2, and θ_1 should be decreased.

The pressure in the piston chamber of the falling period is shown in Figure 14. It can be seen that: ① In the region of (200–224)°, the order of descending rate of the falling period is G4 (15, 20, 68.53), G2 (10, 15, 74.34), G1 (10, 20, 90.10), G3 (10, 25, 103.86), G5 (5, 20, 127.40). The larger θ_1 is, the faster the descending rate is, and θ_1 has the most significant effect on the descending rate of the falling period of the pressure in the piston chamber. Focusing on the three groups of triangular groove parameter combinations G1, G2, and G3 with $\theta_1 = 10°$, it can be found that the larger θ_2 is (θ_3 associated with θ_2 also increases), the slower the descending rate of the falling period. In summary, at this stage, the slot combination G5 is optimal, and θ_2 should be increased as much as possible, while θ_1 should be decreased. ② in the region of (200–224)°, the order of the amplitude of pressure undershoot is G5 (5, 20, 127.40), G2 (10, 15, 74.34), G1 (10, 20, 90.10), G3 (10, 25, 103.86), G4 (15, 20, 68.53). The larger θ_1 is, the smaller the undershoot value is. θ_1 has the most significant effect on the pressure undershoot. Focusing on the three groups of

triangular groove parameter combinations G1, G2, and G3 with $\theta_1 = 10°$, it can be found that the larger θ_2 is (θ_3 associated with θ_2 also increases), the smaller the undershoot value is. In conclusion, the undershoot value of G4 is the smallest at this stage, so the impact of cavitation is also smaller. Therefore, in engineering applications, θ_1 and θ_2 should be increased as much as possible under the allowable conditions of the structure. To sum up, the optimal solutions of these combinations are G1 (10, 20, 90.10) and G3 (10, 25, 103.86).
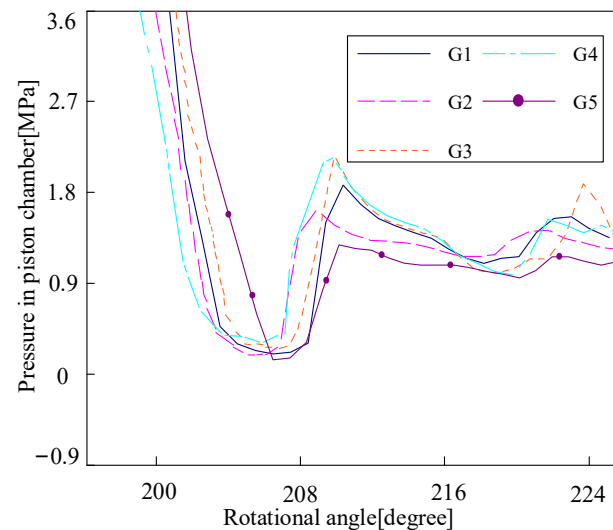

Figure 14. Pressure in the piston chamber with different slot geometries at the beginning of the suction phase.

4.3. Effect of the Working Conditions

In order to investigate the effect of shaft speed on the pressure fluctuation of the piston chamber, the simulations were conducted under the speed of 1000 r/min, 1500 r/min, 2000 r/min, 2500 r/min, and 3000 r/min. Figure 15 shows the pressure in the piston chamber within one period in different speed conditions. It can be seen that: the higher the speed, the greater the pressure fluctuation in the piston chamber. The detailed characteristics of piston chamber pressure during the rising period are shown in Figure 16. It can be seen from the figure that: in this region, the higher the shaft speed, the slower the piston chamber pressure rises. In addition, the pressure curve is delayed when the speed is higher due to the large inertia brought by the high speed.
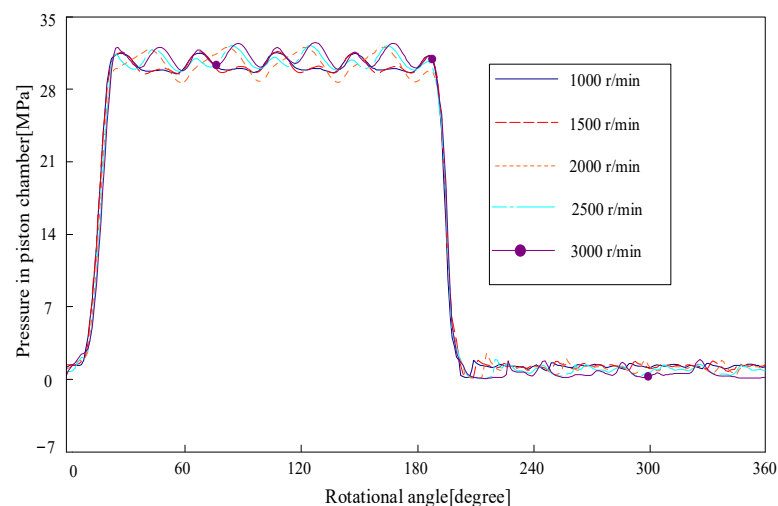

Figure 15. Pressure in the piston chamber with different rotational speeds.
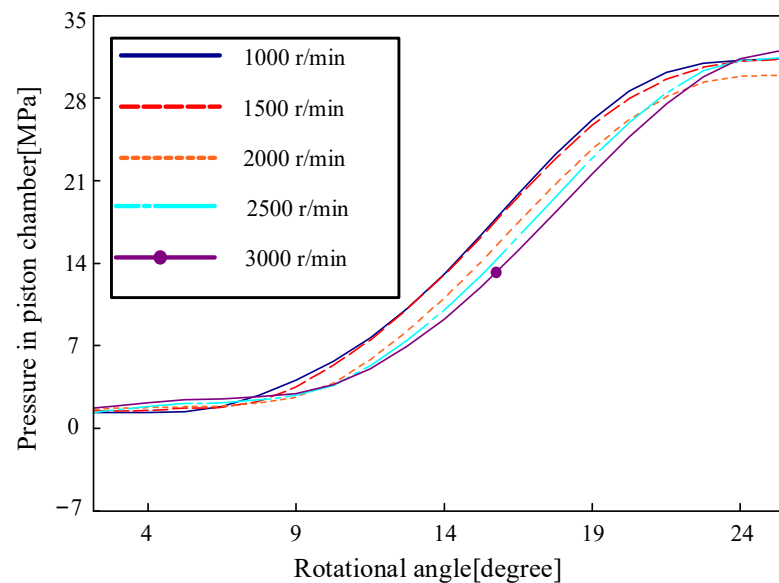
Figure 16. Pressure in the piston chamber with different rotational speeds at the beginning of the discharge phase.

The pressure in the piston chamber of the falling period is presented in Figure 17. As shown in the figure: ① In the (204–228)° region, the lower the shaft speed, the slower the pressure drop of the piston chamber, and there is a small lag. When the piston chamber is connected with the triangular groove of the low-pressure port at a higher speed, the pressure release speed is accelerated; ② At high rotational speed, the undershoot of the piston chamber is significantly higher than that at low rotational speed, which indicates that the increase of rotational speed will accelerate the pressure release process to a certain extent, and maintain the inertia of pressure drop, thus causing greater undershoot.
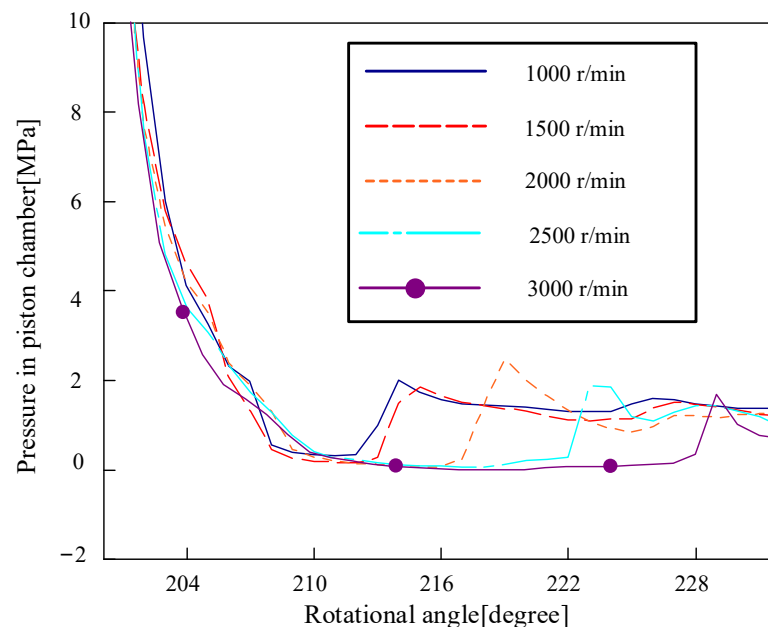

Figure 17. Pressure in the piston chamber with different rotational speeds at the beginning of the suction phase.

The pressure fluctuation curve of the piston chamber under the shaft speed (1000 r/min) and different outlet pressure (12 MPa, 18 MPa, 25 MPa, 30 MPa, 36 MPa) is shown in Figure 18. It can be seen from the figure that: the higher the pressure, the greater the

pressure fluctuation in the piston chamber. The pressure in the piston chamber of the rising period is shown in Figure 19. It can be seen that: In the $(0–24)°$ region, the lower the out pressure, the slower the pressure jump of the piston chamber, and there is a small lag.
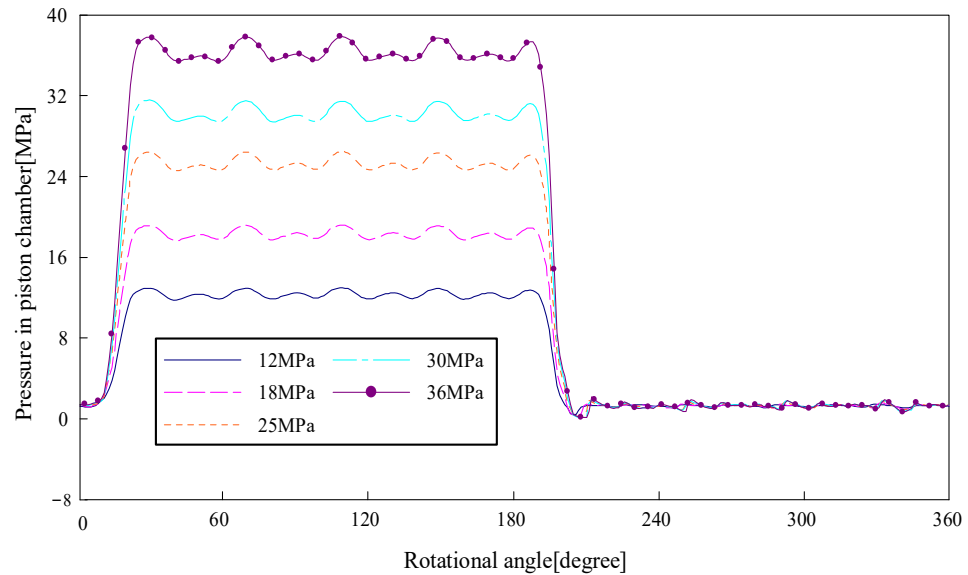

Figure 18. Pressure in piston chamber with different outlet pressure.
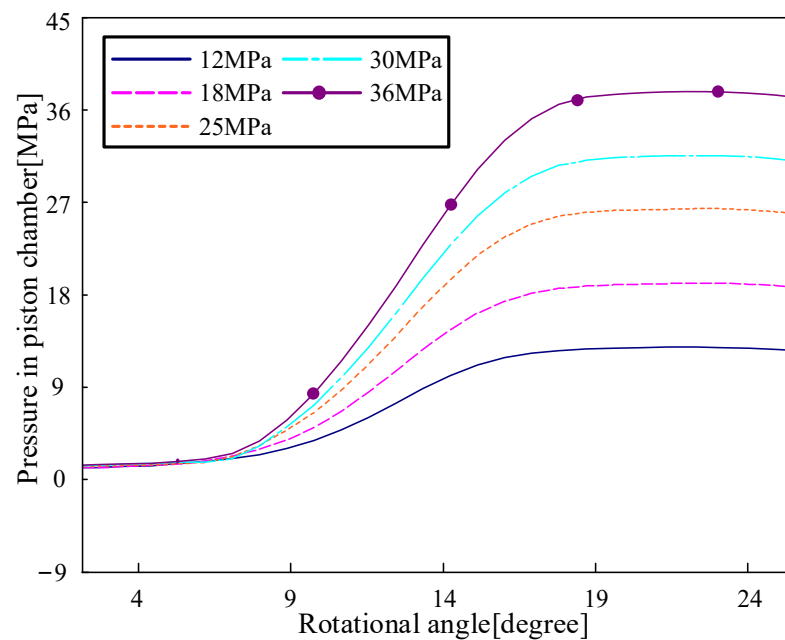

Figure 19. Pressure in the piston chamber with different outlet pressure at the beginning of the discharge phase.

The pressure in the piston chamber of the falling period is shown in Figure 20. It can be seen that: in the $(196–216)°$ area, the higher the outlet pressure, the faster the decline rate, and the amplitude of pressure undershoot is relatively large, which indicates that high outlet pressure is more prone to pressure undershoot. Large pressure undershoot is more likely to cause insufficient suction and air aeration in the fluid and eventually lead to significant cavitation damage in the piston pump. Therefore, it makes sense to reduce the pressure undershoot at the beginning of the suction phase by optimizing the slot geometry of the valve plate.
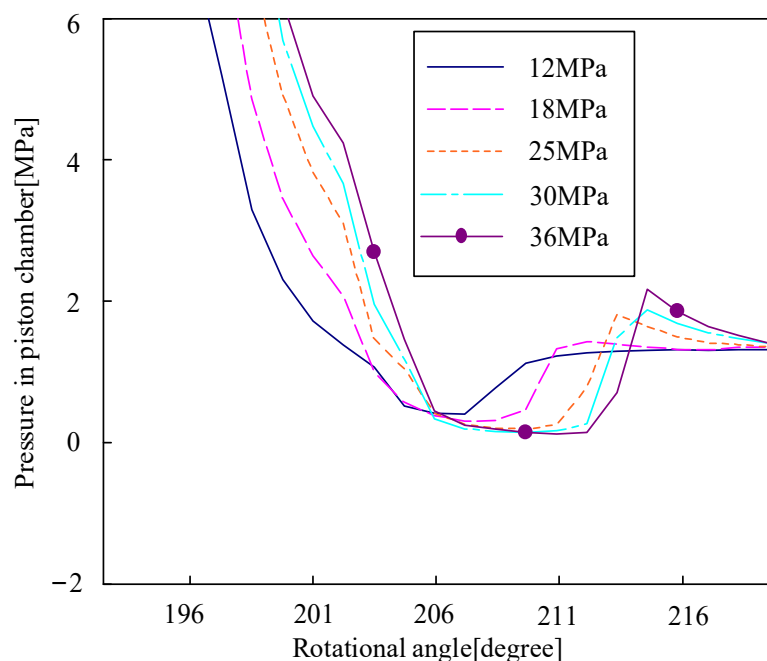
Figure 20. Pressure in the piston chamber with different outlet pressure at the beginning of the suction phase.

5. Conclusions

In this study, a dynamic model of the piston pump was first established, considering the valve plate opening area and leakages of the lubricating interfaces. The mathematical model was verified by comparing the simulated discharge pressure with the test results. Then this verified model was used to investigate the effect of slot geometry and working conditions on the pressure fluctuation in the piston chamber through parametric analysis. The conclusions obtained from further investigations can be summarized as follows:

(1) Among the existing triangular groove parameter combinations, the optimal ones are G1 (10°, 20°, 90.10°) and G3 (10°, 25°, 103.86°). If the volume of the triangular slot remains constant, it would be better to increase θ_2 and θ_1 to reduce the undershoot of the piston chamber pressure in order to avoid cavitation during the transition region;

(2) At different speeds, the overshoot of the pressure in the piston chamber shows no significant difference, while the undershoot of the piston chamber pressure is obviously larger under higher speed conditions. It indicates that increasing the speed will accelerate the pressure release rate and, as a result, aggravate pressure impact and cavitation;

(3) Outlet pressure has a significant effect on the pressure fluctuation of the piston chamber. The fluctuation amplitude and undershoot are higher if increasing the discharge pressure. In actual engineering applications, a large undershoot is more likely to cause cavitation damage at the start-up stage since the outlet pressure not yet reach the maximum value.

This research mainly contributes to a comprehensive understanding of the pressure fluctuation in the piston chamber. Especially, it indicates that optimizing the slot geometry is of great significance in reducing the pressure undershoots during the beginning of the suction phase to avoid cavitation damage.

Author Contributions: Conceptualization, D.W.; methodology, D.W.; software, H.D.; validation, C.C.; formal analysis, H.D.; investigation, C.C.; resources, D.W.; data curation, C.C.; writing—original draft preparation, C.C.; writing—review and editing, H.D.; visualization, D.W.; supervision, D.W.; project administration, D.W.; funding acquisition, D.W. All authors have read and agreed to the published version of the manuscript.

Conflicts of Interest: The authors declare no conflict of interest.

Nomenclature

R	cylinder pitch radius [m]
R_p	piston radius [m]
h_p	average film thickness of piston/cylinder interface [m]
h_s	average film thickness of slipper/swash plate interface [m]
h_v	average film thickness of cylinder block/valve plate interface [m]
β	inclination angle of the swash plate [degree]
φ	angle of the piston relative to the outer dead center [degree]
ω	angular velocity [m/s]
t	Time [s]
n	speed of piston pump [r/min]
L	piston displacement [m]
L_f	coupling length of piston/cylinder interface [m]
u	circumferential speed of the piston [m/s]
d_d	diameter of damping hole of piston ball head [m]
l_d	length of damping hole of piston ball head [m]
d_{in}	inner diameter of slipper sealing belt [m]
d_{out}	outer diameter of slipper sealing belt [m]
v	axial velocity of the piston [m/s]
p	piston chamber pressure [Pa]
p_{case}	housing pressure of piston pump [Pa]
a	axial acceleration of the piston [m²/s]
S_{min}	minimum flow area [m²]
S_S	area of the shaded part [m²]
θ_1	depth angle of transverse section of triangular vibration damping groove [degree]
θ_2	width angle of transverse section of triangular vibration damping groove [degree]
θ_3	width angle of longitudinal section of triangular vibration damping groove [degree]
r	radius of starting and ending circles of kidney groove [m]
z	number of pistons [-]
m	number of piston chamber connected with the high-pressure side of the valve plate [-]
α	piston angular distance [degree]
Q	theoretical oil delivery rate [m³/s]
V_h	volumes of the high-pressure pipeline [m³]
V_1	volumes of the low-pressure pipeline [m³]
$q_{leak,hp}$	leakage flows of the high-pressure port of the valve plate [m³/s]
$q_{leak,lp}$	leakage flows of the low-pressure port of the valve plate [m³/s]
K	volume modulus [-]
$q_{back,hp}$	sum of the backflow of all piston chambers connected with the high-pressure port of the valve plate [m³/s]
$q_{back,lp}$	backflow connected with the low-pressure port of the valve plate [m³/s]
ΔP_{hp}	pressure difference at the orifice of the high-pressure port [Pa]
ΔP_{lp}	pressure difference at the orifice of the low-pressure port [Pa]
Q_t	theoretical displacement of piston pump [m³/r]
C	discharge coefficient [-]
ρ	oil density [kg/m³]
μ	dynamic viscosity of oil [Pa.s]
V_c	volume of oil in piston chamber [m³]
$q_{back,valve}$	backflow when communicating with high-pressure side or low-pressure side of the valve plate [m³/s]
$q_{leaka,piston}$	leakage flow of the piston/cylinder interface [m³/s]

$q_{\text{leaka,slipper}}$	leakage flow of the slipper/swash plate interface [m^3/s]
$q_{\text{leaka,valve}}$	leakage flow of the cylinder block/valve plate interface of the single piston chamber [m^3/s]
R_1	radius of inner oil seal of valve plate [m]
R_2	inner radius of the kidney groove of valve plate [m]
R_3	outside radius of the kidney groove of valve plate [m]
R_4	radius of outside oil seal of valve plate [m]

References

1. Yang, H.Y.; Pan, M. Engineering research in fluid power: A review. *J. Zhejiang Univ. Sci. A* **2015**, *16*, 427–442. [CrossRef]
2. Chao, Q.; Zhang, J.H.; Xu, B.; Huang, H.; Pan, M. A Review of High-Speed Electro-Hydrostatic Actuator Pumps in Aerospace Applications: Challenges and Solutions. *ASME J. Mech. Des.* **2019**, *141*, 050801. [CrossRef]
3. Cho, I.S. A study on the optimum design for the valve plate of a swash plate-type oil hydraulic piston pump. *J. Mech. Sci. Technol.* **2015**, *29*, 2409–2413. [CrossRef]
4. Wang, Y.; Dong, H.K.; He, Y.L. A novel approach for predicting inlet pressure of aircraft hydraulic pumps under transient conditions. *Chin. J. Aeronaut.* **2019**, *32*, 2566–2576. [CrossRef]
5. Chao, Q.; Zhang, J.H.; Xu, B. Centrifugal effects on cavitation in the cylinder chambers for high-speed axial piston pumps. *Meccanica* **2019**, *54*, 815–829. [CrossRef]
6. Dong, H.K.; He, Y.L.; Wang, Y.; Kou, G.Y. Numerical investigation of effect of a centrifugal boost impeller on suction performance of an aircraft hydraulic pump. *Chin. J. Aeronaut.* **2022**, *35*, 236–248. [CrossRef]
7. Zhang, X.; Wu, H.Y.; Chen, C.C.; Wang, D.Y. Oil film lubrication state analysis of piston pair in piston pump based on coupling characteristics of the fluid thermal structure. *Eng. Fail. Anal.* **2022**, *140*, 106521. [CrossRef]
8. Bergada, J.M.; Davies, D.L. The hydrostatic/hydrodynamic behaviour of an axial piston pump slipper with multiple lands. *Meccanica* **2010**, *45*, 585–602. [CrossRef]
9. Zhang, B.; Ma, J.E.; Hong, H.C.; Yang, H.Y. Analysis of the flow dynamics characteristics of an axial piston pump based on the computational fluid dynamics method. *Eng. Appl. Comp. Fluid Mech.* **2017**, *11*, 86–95. [CrossRef]
10. Shah, Y.G.; Vacca, A.; Frosina, E. A fast lumped parameter approach for the prediction of both aeration and cavitation in Gerotor pumps. *Meccanica* **2018**, *53*, 175–191. [CrossRef]
11. Jiang, J.H.; Wang, K.L.; Sun, Y. The Impact of Bushing Thickness on the Piston/Cylinder Interface in Axial Piston Pump. *IEEE Access* **2019**, *7*, 24971–24977.
12. Jiang, J.H.; Wang, Z.B.; Li, G.Q. The Impact of Slipper Microstructure on Slipper-Swashplate Lubrication Interface in Axial Piston Pump. *IEEE Access* **2020**, *8*, 222865–222875. [CrossRef]
13. Zhao, B.; Guo, W.W.; Quan, L. Cavitation of a Submerged Jet at the Spherical Valve Plate/Cylinder Block Interface for Axial Piston Pump. *Chin. J. Mech. Eng.* **2020**, *33*, 67. [CrossRef]
14. Fang, Y.; Zhang, J.H.; Xu, B.; Huang, C.S. A study on increasing the speed limit of axial piston pumps by optimizing the suction duct. *Chin. J. Mech. Eng.* **2021**, *34*, 105. [CrossRef]
15. Chao, Q.; Zi, X.; Tao, J.F.; Liu, C.L. Capped piston: A promising design to reduce compressibility effects, pressure ripple and cavitation for high-speed and high-pressure axial piston pumps. *Alex. Eng. J.* **2023**, *62*, 509–521. [CrossRef]
16. Manring, N.D. Valve-Plate Design for an axial piston pump operating at low displacements. *ASME J. Mech. Des.* **2003**, *125*, 200–205. [CrossRef]
17. Johansson, A.; Olvander, J.; Palmberg, J.O. Experimental verification of cross-angle for noise reduction in hydraulic piston pumps. *Proc. Inst. Mech. Eng. Part I J. Syst. Control. Eng.* **2005**, *221*, 321–330. [CrossRef]
18. Ivantysynova, M.; Seeniraj, G.K. Impact of Valve Plate Design on Noise, Volumetric Efficiency and Control Effort in an Axial Piston Pump. In Proceedings of the ASME 2006 International Mechanical Engineering Congress and Exposition, Chicago, IL, USA, 5–10 November 2006.
19. Seeniraj, G.K.; Ivantysynova, M. Multi-Objective Optimization Tool for Noise Reduction in Axial Piston Machines. In Proceedings of the SAE International Commercial Vehicle Engineering Congress & Exhibition, Rosemont, IL, USA, 7–9 October 2008.
20. Seeniraj, G.K.; Ivantysynova, M. A multi-parameter multi-objective approach to reduce pump noise generation. *Int. J. Fluid Power* **2011**, *12*, 7–17. [CrossRef]
21. Seeniraj, G.K.; Ivantysynova, M. Effect of combining precompression grooves, PCFV And DCFV on pump noise generation. *Int. J. Fluid Power* **2011**, *12*, 53–63. [CrossRef]
22. Wang, S. Improving the Volumetric Efficiency of the Axial Piston Pump. *ASME J. Mech. Des.* **2012**, *134*, 111001. [CrossRef]
23. Ma, J.E.; Fang, Y.T.; Xu, B.; Yang, H.Y. Optimization of Cross Angle Based on the Pumping Dynamics Model. *J. Zhejiang Univ. Sci. A* **2010**, *11*, 181–190. [CrossRef]
24. Xu, B.; Sun, Y.H.; Zhang, J.H.; Sun, T.; Mao, Z.B. A new design method for the transition region of the valve plate for an axial piston pump. *J. Zhejiang Univ. Sci. A* **2015**, *16*, 229–240. [CrossRef]

25. Xu, B.; Ye, S.G.; Zhang, J.H.; Zhang, C.F. Flow ripple reduction of an axial piston pump by a combination of cross-angle and pressure relief grooves: Analysis and optimization. *J. Mech. Sci. Technol.* **2016**, *30*, 2531–2545. [CrossRef]
26. Ye, S.G.; Zhang, J.H.; Xu, B. Noise reduction of an axial piston pump by valve plate optimization. *Chin. J. Mech. Eng.* **2018**, *31*, 31–57. [CrossRef]